

## STATIONKEEPING ANALYSIS FOR SPACECRAFT IN LUNAR NEAR RECTILINEAR HALO ORBITS

Davide Guzzetti<sup>\*</sup>; Emily M. Zimovan<sup>†</sup>; Kathleen C. Howell<sup>‡</sup>; Diane C. Davis<sup>§</sup>

Near Rectilinear Halo Orbits (NRHOs), a subset of the halo orbits characterized by favorable stability properties, are strong candidates for a future inhabited facility in the lunar vicinity. To maintain such orbits in this regime, however, requires a reliable maintenance strategy. Two low-cost, reliable, stationkeeping strategies for maintaining long-term NRHO-like behavior in the ephemeris regime are investigated. Orbit determination errors, orbital perturbations, and spacecraft noise are incorporated into the higher-fidelity simulation environment. As a complement, a real-time warning in the event of a diverging path is presented.

### INTRODUCTION

Since the return of the Apollo 17 spacecraft to Earth in December of 1972, no humans have traveled beyond low Earth orbit. The National Aeronautics and Space Administration (NASA) is focused on a new era of human exploration of the solar system. As a staging ground for such exploration, a current focus of investigation is the development of the capability to sustain a crew in an orbit nearby the Moon. This agenda is also promoted by other international space agencies, as seen in the 2013 Global Exploration Roadmap.<sup>1,2</sup> One of the current orbits of interest as a destination for a habitat spacecraft in cislunar space is a Near Rectilinear Halo Orbit (NRHO). A subset of the halo family of orbits, the NRHOs are attractive as staging orbits for several reasons, including advantageous transfers from Earth and to destinations beyond the Earth's vicinity, availability of communications links, the potential to limit time in eclipse, and favorable access to the lunar surface.<sup>3</sup>

The current investigation explores the feasibility of an Earth-Moon NRHO as a destination for a crewed spacecraft in a long-term orbit in cislunar space from the perspective of orbit maintenance. As are many libration point orbits, the NRHOs are sensitive to perturbations and, thus, a stationkeeping scheme is required to ensure a spacecraft remains in an NRHO long-term. While multiple robotic missions—including ACE, SOHO, WIND,<sup>4</sup> WMAP,<sup>5</sup> GENESIS,<sup>6</sup> and JWST,<sup>7</sup> which exploited Sun-Earth libration point orbits, and ARTEMIS,<sup>8</sup> the first Earth-Moon libration point orbiter—successfully implemented stationkeeping algorithms in both analysis and operations, the NRHO regime is less explored from an orbit maintenance perspective. In addition, maintaining a manned spacecraft offers additional challenges in the form of orbital perturbations due to a human presence, for example, expulsion of waste products. To validate the NRHO as a viable destination for a habitat spacecraft, cost-effective stationkeeping algorithms must be identified that will maintain the spacecraft reliably in orbit within the available  $\Delta V$  budget.

Various approaches to orbit maintenance may be developed as a response to competing requirements. For example, identifying the cheapest stationkeeping solution, in terms of propellant costs, may require significant numerical effort. However, a maintenance strategy that requires a smaller computational load may be beneficial for a successful on-board implementation, rapid correction of errors that may be hazardous to the

<sup>\*</sup>Ph.D. Candidate, School of Aeronautics and Astronautics, Purdue University, Armstrong Hall of Engineering, 701 W. Stadium Ave., West Lafayette, IN 47907-2045.

<sup>†</sup>Graduate Student, School of Aeronautics and Astronautics, Purdue University, Armstrong Hall of Engineering, 701 W. Stadium Ave., West Lafayette, IN 47907-2045. Member AAS; Member AIAA.

<sup>‡</sup>Hsu Lo Distinguished Professor, School of Aeronautics and Astronautics, Purdue University, Armstrong Hall of Engineering, 701 W. Stadium Ave., West Lafayette, IN 47907-2045. Fellow AAS; Fellow AIAA.

<sup>§</sup>Principal Systems Engineer, a.i. solutions, Inc., 2224 Bay Area Blvd., Houston, TX, 77058, USA. Member AAS.

human crew, or to offset an escaping path. Dynamical systems theory is applied to exploit an understanding of the dynamics in the NRHO regime, allowing for smaller computational loads, through an exploration of stationkeeping via the Cauchy-Green Tensor (CGT). Alternatively, stationkeeping methodologies previously applied to robotic libration point orbiters are adapted to the NRHO to explore costs associated with corrections of additional errors related to a noisy, human-crewed spacecraft. Considering the many uncertainties in the current mission definition, demonstrating multiple strategies that can successfully maintain NRHO motion is very useful. Development of an optimal stationkeeping method from a cost perspective is not pursued in this investigation, rather, the focus is on the generation of multiple maintenance strategies in response to various mission objectives.

## DYNAMICAL MODELS

To develop a stationkeeping process for lunar near rectilinear halo orbits, dynamical models that offer different levels of fidelity are employed. The Circular Restricted Three-Body Problem (CR3BP) provides an autonomous approximation to Earth-Moon dynamics, enabling an understanding of underlying dynamical structures. The ephemeris model allows for higher-fidelity simulations.

The CR3BP dynamical model serves as a reasonable approximation to higher-fidelity dynamical models in the Earth-Moon system. Within this application of the CR3BP, the motion of a massless spacecraft under the gravitational influence of the Earth and Moon is considered. These two primary bodies, modeled as point-masses, are assumed to move in circular orbits about their common barycenter. The motion of the spacecraft is then described relative to a coordinate frame that rotates with the motion of the Earth and Moon. By convention, quantities in the CR3BP are nondimensionalized such that the Earth-Moon distance, as well as the mean motion of the primaries, are both equal to a constant value of unity. In addition, the Earth and Moon have nondimensional masses equal to  $1 - \mu$  and  $\mu$ , respectively, where the parameter  $\mu$  equals the ratio of the mass of the Moon to the total mass of the system. The CR3BP admits five relative equilibrium points: the collinear points  $L_1$ ,  $L_2$ , and  $L_3$ , located along the Earth-Moon line, and two equilateral points,  $L_4$  and  $L_5$ , forming equilateral triangles with the two primaries. Since the CR3BP is autonomous, a constant energy integral exists relative to the rotating frame and is defined as the Jacobi constant, such that  $JC = 2U - v^2$ , where  $U$  is the pseudo-potential function and  $v$  is the velocity magnitude relative to the rotating frame.<sup>9</sup>

For applications to actual mission scenarios where high-fidelity modeling accuracy is required,  $N$ -body differential equations and planetary ephemerides are employed. The  $N$ -body dynamics generally render the motion of a particle of interest (e.g., a spacecraft) in an inertial frame relative to a central body under the gravitational influence of the same central body and other additional perturbing particles. Within this analysis, the relative position of each perturbing body with respect to the central body is instantaneously computed by employing NAIF SPICE ephemeris data. The Moon is selected as the central body for numerical integration in the J2000 inertial frame. The Earth, Moon, Sun, and Jupiter are incorporated in the  $N$ -body ephemeris model. For additional resolution in some simulations, the Moon's gravity is modeled using the GRAIL (GRGM660PRIM) model truncated to degree and order 8.

## NEAR RECTILINEAR HALO ORBITS

Near rectilinear halo orbits<sup>10</sup> in the vicinity of the Moon are identified as potential long-term orbits for a crewed vehicle in the cislunar region. The NRHOs offer advantages such as relatively inexpensive transfer options from the Earth, feasible transfer options to the lunar surface as well as other orbits in cislunar space and beyond, and advantageous eclipsing properties.<sup>3,11</sup> Comprising a portion of the larger family of  $L_2$  halo orbits, depicted in Figure 1(a), the NRHO subset can be approximately bounded by specific locations reflecting changes in the linear stability across the  $L_2$  halo family; these bifurcation orbits are indicated in red and by colored arrows in Figure 1(a).

### Stability

Within the context of the CR3BP, it is relatively straightforward to determine the linear stability associated with periodic orbits. Linear stability for a periodic solution in any autonomous dynamical system is assessed by the eigenvalues of the State Transition Matrix (STM) evaluated after precisely one periodic interval, i.e.,

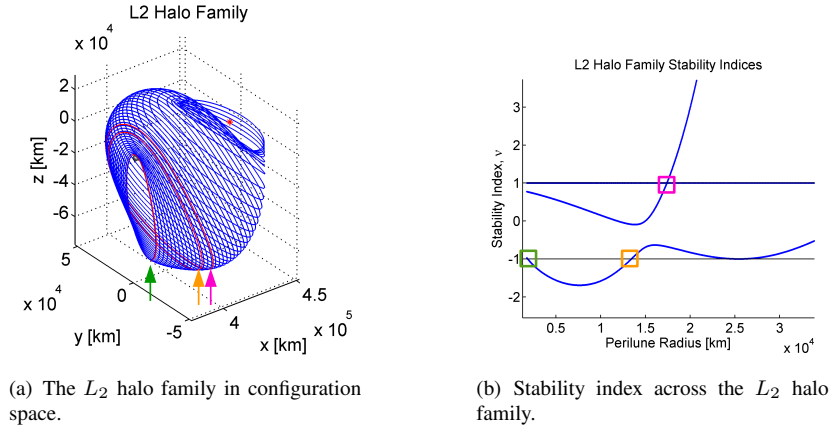


**Figure 1:** Definition of NRHO segment for the  $L_2$  halo family within the Earth-Moon system (CR3BP).

the monodromy matrix. The STM is essentially a linear mapping and reflects the convergence or divergence of variations relative to a reference solution. Two well-known properties of the monodromy matrix, as applied within the context of the CR3BP, are necessary to analyze the stability of NRHOs: (1) The eigenvalues of the monodromy matrix always appear in reciprocal pairs, and (2) one pair of eigenvalues is always equal to unity due to the periodicity of the orbit and the existence of a family of such orbits with precisely periodic behavior. Excluding the trivial pair, two reciprocal pairs of eigenvalues,  $(\lambda_i, 1/\lambda_i)$ , may be combined into a single metric for the purpose of describing the stability of the corresponding mode. A stability index is then defined as  $\nu_i = \frac{1}{2} (\lambda_i + 1/\lambda_i)$  for  $i = 1, 2$ . If the stability indices,  $\nu_i$ , are both less than one in modulus, then the orbit is marginally stable in a linear sense; the orbit is otherwise unstable. For a diverging path, a larger value of the stability index corresponds to a faster departure from the reference.

The linear stability characteristics associated with the halo family in the CR3BP serve to delineate the NRHO boundaries. Within the  $L_2$  halo orbit family, the NRHOs are identified as a specific segment within the family between two distinct markers. Across the family in the region of interest near the smaller primary, three stability switches—a transition from marginally stable to unstable or vice versa—are indicated by colored arrows in Figure 1(a). Thus, for the purpose of this investigation, an  $L_2$  NRHO is defined within the Earth-Moon system as a halo orbit between the first and third stability changes, marked with green and pink arrows in Figure 1(a) and green and pink boxes in Figure 1(b). This definition equivalently applies to both the northern and southern members of the  $L_2$  halo family. Geometry also distinguishes an NRHO from the larger set of halo orbits; the NRHOs are characterized by an elongated shape that resembles an ellipse when it is plotted in the CR3BP rotating frame; the orbits are also dominated by their out of plane component. Earth-Moon  $L_2$  NRHOs are characterized by perilune radii ranging from approximately 1850 km to 17350 km. The orbital periods of the  $L_2$  NRHOs range from about 6 days to just over 10 days.

The NRHOs corresponding to stability indices  $|\nu_i| > 1$  are unstable. The divergence rate is, however, significantly slower than other halo orbits that are closer to the  $L_2$  Lagrangian point, as evaluated in the Earth-Moon system. The temporal scale for the instability is roughly predicted by the modulus of the stability index. When both the stability indices are close to unity in modulus, such as for an NRHO, divergence is slow. Within the NRHO range, both stability indexes remain bounded and nearly equal to one. A reference metric for the temporal scale of the dominant diverging motion may be derived by considering the time constant,  $\tau$ , as measured in number of revolutions for the nominal orbit, defined as

$$\tau[\text{rev}] = \frac{1}{\text{Re}(\ln(\lambda_{\max}(\Phi(P, 0))))} \frac{1}{P} \quad (1)$$

where  $\lambda_{\max}(\cdot)$  is an operator that returns the largest eigenvalue of the argument matrix,  $\Phi(P, 0)$  denotes the STM over precisely one period of the orbit, and  $P$  is the period of the corresponding orbit. Note that the time constant is infinite for a marginally stable orbit, i.e.,  $\lambda_{\max}(\Phi(P, 0)) = 1$ . The value  $\tau$  is interpreted as the time necessary to amplify a given initial perturbation by a factor of approximately 3, assuming that the growth is proportional to the exponential function  $e^{\frac{t[\text{rev}]}{\tau[\text{rev}]}}$ . The time constant associated with NRHOs is

displayed in Figure 2. Favorable stability properties and the time scale of divergence within the CR3BP suggest the possibility of maintaining NRHO motion for a long duration while consuming few propellant resources. Leveraging this opportunity requires the introduction of a stationkeeping algorithm to maintain NRHO-like motion in a higher-fidelity environment.

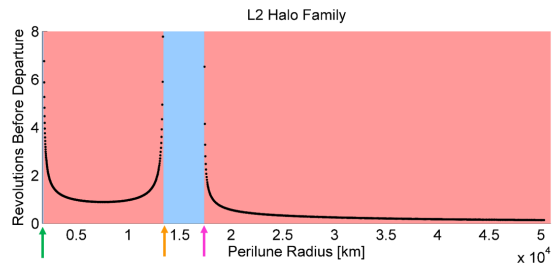


**Figure 2:** Linear time constant for the  $L_2$  NRHO region within the Earth-Moon system. Blue regions indicate marginally stable orbits, red regions indicate unstable orbits. Colored arrows correspond to the marked red orbits in Figure 1(a).

### Apse Angle

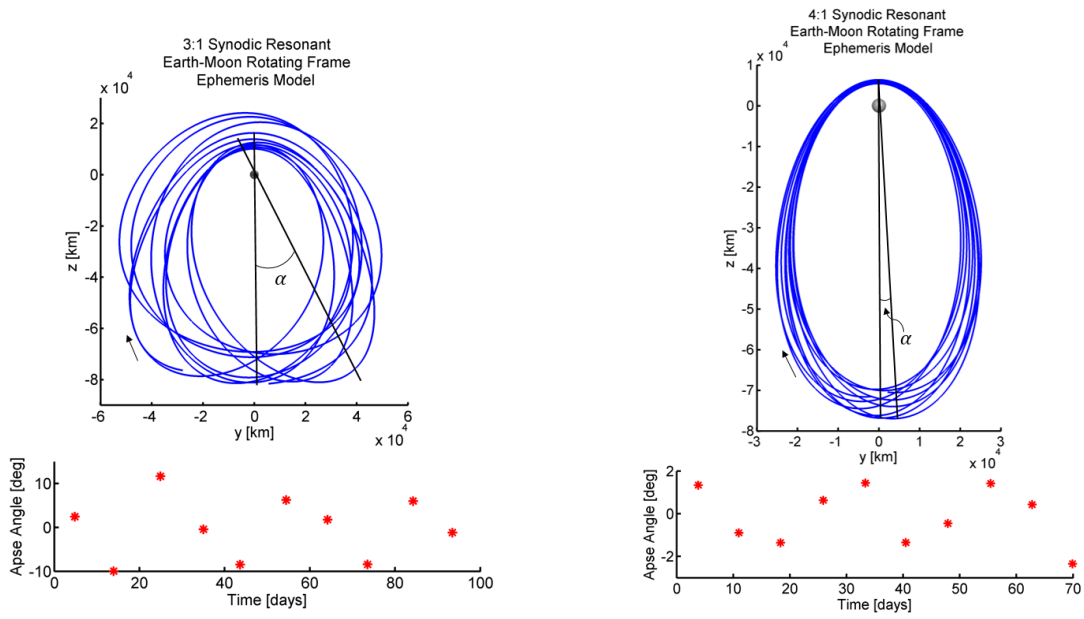
Given periodic NRHOs in the CR3BP, transition to a higher-fidelity ephemeris force model yields quasi-periodic motion. The transition can result in either “tight,” nearly-periodic orbits or “loose,” more variable revolutions along a trajectory. A metric is defined for convenience to describe the spread of the orbit from a perfectly periodic CR3BP analog. The metric is denoted the apse angle,  $\alpha$ , and is depicted in Figure 3. The apse angle reflects how closely each revolution along an ephemeris trajectory mirrors the previous revolution or the evolution of an ephemeris trajectory relative to a periodic CR3BP NRHO in terms of orientation in the  $yz$ -plane. By definition, a CR3BP periodic NRHO retains a constant apse angle,  $\alpha = 0^\circ$ . The apse angle is evaluated as the osculating argument of periapsis, as computed at the closest approach of the ephemeris trajectory relative to the Moon, minus  $90^\circ$ ; thus, it is evaluated once every revolution. Figure 3(a) reflects the fact that the apse angle along a converged ephemeris trajectory can vary widely, as illustrated by the 3:1 synodic resonant NRHO converged using only a continuity constraint. Alternatively, as apparent in Figure 3(b), some ephemeris NRHOs closely resemble their CR3BP counterparts. Additionally, since the NRHOs in Figures 3(a) and 3(b) are, in fact, a 3:1 synodic resonant orbit and a 4:1 synodic resonant orbit, respectively, some cyclic behavior in apse angle can be observed in the plots of  $\alpha$  in Figures 3(a) and 3(b). The plots also serve to identify the resonances when visual inspection, e.g., in Figure 3(a), may not reveal obviously repeating behavior.

### Escape Warning

In a human spaceflight application, monitoring the effects of perturbations on the planned path is vital to the timing of correction maneuvers and to ensure crew safety. A significant consideration also explored in this investigation is the potential to anticipate, or predict, an escaping path. An escape warning is useful, particularly if escape can be predicted prior to any visual evidence of any apparent diverging states. Thus, defining a simple quantity to detect an escape with a sufficient time margin can be a key capability. Initially, consider the following scalar quantity along a trajectory constructed in the CR3BP, i.e.,

$$\text{MI}_\Gamma(t) = \int_{t_0}^t x(\tau)\dot{x}(\tau) + y(\tau)\dot{y}(\tau) + z(\tau)\dot{z}(\tau)d\tau \quad (2)$$

where  $x, y, z$  are the position coordinates relative to the rotating frame and  $\dot{x}, \dot{y}, \dot{z}$  are the corresponding velocity components, which are functions of a single independent time variable,  $\tau$ . The expression in Eq. (2) is effectively a line integral for the position vector field computed between the initial epoch,  $t_0$ , and current epoch,  $t$ . For convenience, the quantity defined in Eq. (2) is termed the momentum integral. The momentum integral along a closed orbit is equal to the circulation of the position vector as observed in the CR3BP rotating frame. For a trajectory that is periodic with respect to the CR3BP rotating frame, the momentum integral

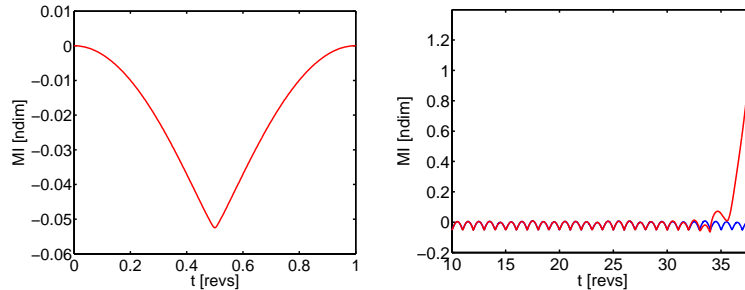


(a) An ephemeris trajectory with a wider spread relative to a corresponding CR3BP orbit, as determined by the large range of the apse angle and the “loose” appearance in the Earth-Moon rotating frame.

(b) An ephemeris trajectory with a narrow spread that remains close to a corresponding CR3BP orbit, as determined by the small range of the apse angle and the “tight” appearance in the Earth-Moon rotating frame.

**Figure 3:** Computation of the apse angle to quantify the evolution of a converged ephemeris trajectory in comparison to a corresponding CR3BP NRHO.

is null when it is computed over one period as follows from the fundamental theorem of calculus. As an example, the momentum integral evolves along a CR3BP NRHO with perilune radius equal to 3500 km, and returns to zero after one revolution of the orbit, as demonstrated in Figure 4(a). Within the present analysis,



(a) Momentum integral along an NRHO in the CR3BP over one revolution.

(b) Representative time history for the momentum integral along a trajectory in the ephemeris model.

**Figure 4:** Momentum integral in the CR3BP (a) and ephemeris model (b)

the integral in Eq. (2) is solved numerically by applying the trapezoid rule with a small integration step along a numerically constructed reference path. The momentum integral may also be evaluated for an ephemeris trajectory; as an ephemeris trajectory is not likely to precisely return to the initial state, the momentum integral is not expected to be zero after each revolution. However, the momentum integral is bounded if the orbital motion is bounded.

Comparing the momentum integral profile for a baseline trajectory to a slightly perturbed path that departs from the reference orbital path illustrates the evolution of the momentum integral over many revolutions. For this scenario, the time history for the momentum integral is plotted in Figure 4(b). The blue curve, repre-

sending the nominal path, is bounded and approximately repeats over each revolution. The red curve reflects the perturbed trajectory. After approximately 30 revolutions, the perturbed path begins diverging. As the departure evolves, the momentum integral profile is no longer bounded and does not approximately repeat over each revolution of the nominal orbit.

Observing the two curves in Figure 4(b), a good metric to detect divergence is the instantaneous difference between the momentum integral computed for a perturbed trajectory versus a given long-term baseline trajectory. The difference is defined as

$$\Delta MI(t) = \log |MI_{\tilde{\Gamma}}(t) - MI_{\Gamma}(t)| \quad (3)$$

where  $\tilde{\Gamma}$  refers to the perturbed trajectory and  $\Gamma$  refers to the reference orbit; a logarithm function is introduced to reveal the order of magnitude for the momentum integral difference. For the difference in Eq. (3) to be valid, the momentum integral for the reference trajectory,  $MI_{\Gamma}(t)$ , and for the perturbed orbit,  $MI_{\tilde{\Gamma}}(t)$ , must be evaluated originating from the same initial state and epoch. Since the metrics  $MI_{\Gamma}(t)$  and  $MI_{\tilde{\Gamma}}(t)$  are integral, or cumulative, quantities, they conserve any initial discrepancy. If the momentum integrals  $MI_{\Gamma}(t)$ , and  $MI_{\tilde{\Gamma}}(t)$  are computed from different initial conditions, the resulting profiles are offset by a constant bias and, possibly, a phase difference.

A valid instantaneous variation, along a logarithmic scale, for a perturbed momentum integral (red curve in Figure 4(b)) relative to a baseline profile (blue curve in Figure 4(b)) appears in Figure 5(a). When the orbital motion begins diverging, the order of magnitude of  $\Delta MI$  rises quickly. In Figure 5(a), the vertical line indicates where the osculating eccentricity relative to the Moon is equal to unity. At the moment when

the lunar osculating eccentricity is unitary, the trajectory has already diverged from the reference NRHO, and a  $\Delta V$  to recover the desired motion near the Moon may be excessively large. As a rule of thumb, the diverging path should be corrected, at minimum, 3-4 revolutions prior to the osculating eccentricity relative to the Moon reaching a unitary value. Advance anticipation of the correction maneuver may be beneficial in terms of crew safety and propellant cost. Monitoring of the momentum integral difference offers a valid means to predict, with a sufficient time margin, the divergence of the current trajectory relative to the baseline motion. A threshold on the difference in the momentum integral,  $\Delta MI$ , can be employed to indicate divergence. In this case, the horizontal dashed line marks a threshold that indicates the initiation of divergent behavior from the baseline path. As a proof of concept, Figure 5(b) depicts the warning margin between escape detection using the momentum integral difference and that using osculating eccentricity over multiple trials. The advance warning based on the momentum integral difference is between four and six revolutions.

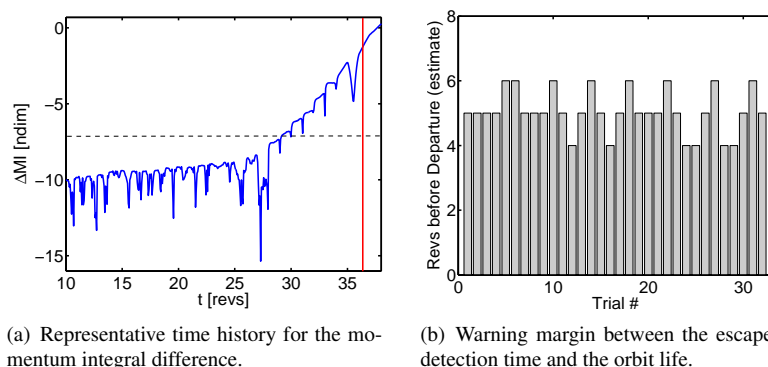


**Figure 5:** Escape prediction using the momentum integral difference.

## STATIONKEEPING FOR LIBRATION POINTS ORBITS: PREVIOUS CONTRIBUTIONS

There exists a relatively large collection of previous investigations concerning control of libration point orbits. Such reports often elaborate on existing strategies for application to a specific stationkeeping problem in a multi-body regime, or combine pieces from different procedures to create an alternative approach. Therefore, it is not straightforward to uniquely classify previous contributions into a rigid list of possible stationkeeping techniques. While the following summary is not all-inclusive, and some methods may partially overlap or combine, it is representative of some recent trends that are useful for stationkeeping for libration point orbits:

1. *Classical Control Theory*.<sup>12–16</sup> Methods from classical control theory are adapted and applied to the stationkeeping problem in a multi-body regime.
2. *Floquet Mode Control*.<sup>9,17–21</sup> Stationkeeping maneuvers are designed to cancel the unstable mode for a reference solution or otherwise leverage knowledge of the invariant structures.
3. *Target Point*.<sup>19,20,22–24</sup> Specific future position and velocity states (i.e., target points) along a pre-computed reference trajectory are targeted.
4. *Hamiltonian Preserving Strategy*.<sup>9,21,25</sup> An artificial, instantaneous center manifold is created to maintain a spacecraft in oscillatory motion nearby a reference trajectory. The maneuver is constructed by combining the projections of the position error along the unstable and stable local, instantaneous modes.
5. *Continuation Strategy*.<sup>26–28</sup> Each maneuver is determined to ensure the continuation of the orbit for several revolutions downstream or to achieve some specific parameter values that are then targeted downstream, for example, energy level, osculating orbital elements, epoch, or position and velocity states. The underlying theme is leveraging the asymptotic behaviors of the natural dynamics.
6. *Crossing Control*.<sup>14,29–31</sup> Maneuvers are designed to control conditions at the next crossing of some orbit near-symmetry plane. It is a common practice to target an approximate perpendicular crossing of the  $xz$ -plane within the instantaneous CR3BP rotating frame (i.e., limit the rotating  $x$ -velocity component at the plane crossing).

For this current application involving a crewed vehicle, a stationkeeping strategy to maintain the behavior in an NRHO is constructed through the understanding of previously successful approaches while solving specific challenges that are associated with NRHO dynamics within the Earth-Moon system.

## STATIONKEEPING FOR NEAR RECTILINEAR HALO ORBITS

Previous robotic mission applications, such as ARTEMIS<sup>26</sup> and GENESIS,<sup>22</sup> along with other simulated scenarios, have demonstrated that employing a virtual baseline and selecting a target state that is located a certain number of revolutions downstream may be beneficial. A “virtual baseline” broadly refers to the concept of targeting a type of reference motion rather than a specific, fixed trajectory that is pre-planned from the initial to final epoch. A virtual baseline also allows opportunities for updates of the reference to maintain the validity of linear variational strategies. Targeting further downstream leverages the long-term natural flow to achieve a desired final state. A virtual baseline may simplify stationkeeping operations particularly since targeting long horizon goals may reduce the  $\Delta V$  cost. A single-step stationkeeping approach can serve to both generate this virtual baseline and target the baseline in one step. A typical implementation plan for a single-step approach to stationkeeping includes: the selection of a CR3BP solution as an initial guess to a corrections algorithm; the definition of target conditions many revolutions downstream along the orbit; the application of orbit determination errors; and, the numerical correction of the motion within a higher-fidelity ephemeris model. Thus, the single-step stationkeeping approach basically achieves three goals: (1) generates a ballistic motion in an ephemeris model, (2) acquires a long horizon target state, and (3) compensates for orbit determination errors.

Significant challenges exist in applying the single-step algorithm to generate an NRHO-like motion in a higher-fidelity model. Recall that, as members of halo families of orbits, NRHOs are characterized by sensitive dynamics that are numerically challenging in simulations. These orbits also pass very near a primary and possess high osculating eccentricity values with relatively large variations in speeds over each revolution. In this regime, the perturbations in a higher-fidelity model may be near the same frequency as the fundamental dynamical modes.<sup>32,33</sup> As a consequence, high-cost trajectories, in terms of  $\Delta V$ , may exist nearby low-cost solutions, and numerical algorithms that are based on linear approximations of the dynamics nearby the reference, such as gradient-based methods, may struggle to compute a suitably low-cost route. As noted, simulating the motion within a higher-fidelity regime, such as the N-body ephemeris model, adds an additional level of complexity. The stationkeeping algorithm for NRHOs may require, therefore, more guidance to be adequately effective. A single-step approach to stationkeeping is also computationally intensive (and ill-suited for on-board applications) because it re-converges the ballistic solution at each maneuver. Reproducing a large number of single-step simulations, for example in a Monte Carlo analysis, is less practical

as it generally requires a longer computation time. Additionally, targeting a long horizon state or condition to compensate for small orbit determination errors may not significantly reduce the overall  $\Delta V$  costs, and re-converging the long term component of the motion may be redundant.

To compensate for difficulties in applying a single-step algorithm, the goals for a stationkeeping strategy can be separated into successive steps. Consider a two-step procedure. At the first level, a maneuver that implements an NRHO virtual baseline and achieves long horizon objectives is generated. A CR3BP trajectory is employed as an initial guess for the virtual reference. Within the given tolerance and current higher-fidelity model, the resulting trajectory is ballistic, i.e., no additional maneuvers following the initial burn are required and no perturbations are included. The first level is denoted as the Long Horizon (LH) maintenance step. Essentially, LH maintenance yields updated baselines as necessary. On a second level, perturbations to the nominal motion are added, and a corrections strategy to maintain the orbit sufficiently close to the virtual reference is implemented. Maneuvers are inserted to compensate for orbit determination errors. Each maneuver is computed to target a vector or scalar state, or a condition, downstream. Because a downstream target is only one or a few revolutions ahead of the current state, this level is termed Short Horizon (SH) maintenance. Target states for the SH level are supplied by the long-term virtual ephemeris motion obtained in the LH level.

Decomposing the stationkeeping procedure into two steps offers some benefits. Using SH maneuvers to compensate for orbit determination errors and other small perturbations is computationally efficient. For small variations along the virtual reference, simple corrections algorithms (e.g., single shooting methods) may be employed. The long-term virtual baseline is only updated when it is strictly necessary using LH maneuvers. Any post-insertion maneuver may be implemented as an LH burn, and may benefit from the cost reduction that is generally granted by targeting many revolutions downstream along the path. Figure 6 displays schematics for the orbit maintenance strategy as split into LH and SH levels. To summarize, the

scope of an LH maneuver is to set the spacecraft on a path that generally resembles a specified CR3BP motion within the ephemeris model that meets the mission requirements. An LH maneuver may be useful for extending the orbit life, avoiding an eclipse, shifting the reference

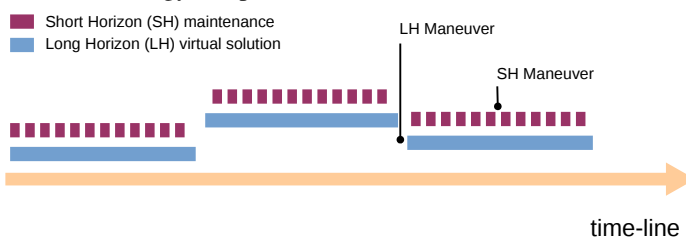


**Figure 6:** Orbit maintenance strategy schematic.

Following an LH maneuver, SH maneuvers serve to compensate for recurring orbit determination errors and other small perturbations, such as a noisy spacecraft. Both LH and SH maneuvers are generally necessary to maintain an NRHO in an actual mission application.

## Long Horizon Maneuvers

A variety of algorithms may be employed to compute LH maneuvers. Since LH maneuvers are computed less frequently than SH maneuvers, increases in computational cost (as occurs, for example, in optimization) are less critical. A possible framework for an LH maintenance algorithm is described by the following steps.

1. **Introduce input:** A solution in the CR3BP supplies an accurate initial guess for an NRHO-like motion in the ephemeris model. Let  $\phi_{3B}(\mathbf{x}, t)$  be the dynamical flow associated with the CR3BP equations of motion. Let the vector  $\mathbf{x}_0$  represent the position and velocity states. Then, any state,  $\mathbf{x}_0$ , that belongs to an NRHO periodic orbit, denoted  $\Gamma_{NRHO}$ , satisfies  $\mathbf{x}_0 = \phi_{3B}(\mathbf{x}_0, P)$  for  $\mathbf{x}_0 \in \Gamma_{NRHO}$ , where time  $t = P$  is the period of the orbit. The above relationship is also satisfied for any integer multiple of the period.
2. **Generate patch points:** A discrete set of states (position and velocity), denoted patch points, is selected along a full revolution of the CR3BP periodic orbit. A common discretization for a trajectory is the adoption of patch points equally spaced in time. These patch points serve to converge a solution in the ephemeris model. Let  $\mathbf{x}_i = [x; y; z; \dot{x}; \dot{y}; \dot{z}]_i$  be the state vector, within the CR3BP, corresponding to the time instant  $t_i \in [0, P]$ , such that  $\mathbf{x}_i \in \Gamma_{NRHO}$ . Then, the complete set of variables for  $n$  patch

points over one revolution is written as

$$\mathbf{X}_{3B}^{r1} = [\mathbf{x}_1 \quad \mathbf{x}_2 \quad \dots \quad \mathbf{x}_n]^T \quad (4)$$

with  $t_i = (i - 1)P/n$ , for  $i = 1, \dots, n$ . The state variable vector constructed within the CR3BP,  $\mathbf{X}_{3B}^{r1}$ , supplies a good initial guess for the corrections process in the ephemeris model.

3. **Duplicate patch points:** The CR3BP periodic orbit is reproduced for a given number of revolutions,  $N_{rev}$ . The patch points vector,  $\mathbf{X}_{3B}^{r1}$ , is cloned  $(N_{rev} - 1)$  times, and stacked, to create an initial guess for  $N_{rev}$  revolutions of the orbit,

$$\mathbf{X}_{3B} = [\mathbf{X}_{3B}^{r1} \quad \mathbf{X}_{3B}^{r1} \quad \dots \quad \mathbf{X}_{3B}^{r1}]^T \quad (5)$$

with a time vector

$$\mathbf{t} = \left[ 0, \frac{P}{n}, \frac{2P}{n}, \dots, P, P + \frac{P}{n}, \dots, (N_{rev} - 1)P, \dots, (N_{rev} - 1)P + \frac{P}{n}, \dots, (N_{rev} - 1)P + \frac{(n-1)P}{n} \right]$$

rendering the epoch for each patch point in the series. For convenience,  $\mathbf{X}_{3B}$  is also converted into the J2000 frame, yielding  $\mathbf{X}_{J2000}$ . Similarly, the time vector is converted into an array of epochs,  $\mathbf{E}_{J2000} = E_0 + \mathbf{t}$ , where  $E_0$  denotes the selected initial epoch. The patch point vector,  $\mathbf{X}_{J2000}$ , and the epoch array,  $\mathbf{E}_{J2000}$ , are used to propagate the trajectory within the ephemeris model.

4. **Define constraints:** Possible constraints along the path are then introduced into the process. Constraints are used to render specific orbit conditions at selected epochs or patch points. Typically, constraints are applied at the beginning or end on a trajectory arc, however, constraints on intermediate patch points are also possible. If a desired constraint applies to a location that is not included in the original set of patch points, it may be necessary to add a patch point at the location where the orbit constraint is required. Assigning the initial position and/or epoch is a common constraint. Fixed initial spacial coordinates may, for example, describe an insertion location into an orbit, or some specific position for a post-insertion maneuver to extend the orbit life. Assigning an initial epoch may represent a phasing constraint. Note that any constraint must be expressed consistent with the corrections algorithm formulation. For example, if the corrections algorithm utilizes a J2000 reference system, constraints that are formulated within the CR3BP rotating coordinates must be transformed to equivalent constraint equations in the J2000 frame.
5. **Converge motion in ephemeris:** Using a corrections algorithm, e.g., multiple shooting,<sup>34</sup> the patch point vector,  $\mathbf{X}_{J2000}$ , and epoch vector,  $\mathbf{E}_{J2000}$ , are iteratively adjusted to obtain a solution within the ephemeris model that is continuous and that satisfies the constraints. Both internal continuity and user-defined constraints are achieved within a given tolerance. A convergence tolerance is selected to enable the correct functioning of the SH level while avoiding excessive numerical precision at this level. Tightening the tolerance more than necessary increases the computational load, and errors introduced in the SH level reduce the need for extremely high accuracy. A tolerance of  $10^{-6}$  nondimensional units, which is equivalent to approximately 0.380 km for position and 0.1 cm/s for velocity, is generally a good compromise between computational time and solution accuracy for the LH level for the NRHOs.
6. **Deliver output:** The corrected patch point vector,  $\mathbf{X}_{J2000}$ , and epoch vector,  $\mathbf{E}_{J2000}$  are the output for the LH level, and may be propagated numerically to render the desired motion in the ephemeris model to within the selected tolerance.

For the application of sustaining NRHO-like motion in the ephemeris environment, an LH maneuver generates a path that retains the general characteristics of a trajectory that is identified within the CR3BP. In higher-fidelity simulation, LH maneuvers are also useful to introduce large modifications from the reference, for example, maneuvers that are required to extend orbit life, avoid an eclipse, correct for a missed burn, or offset a potential escape from the system.

### Short Horizon Maneuvers

Short Horizon (SH) maneuvers are introduced to correct orbit determination errors, and small perturbations to the virtual reference that is supplied by an LH maneuver. Two algorithms are investigated for the efficient

computation of SH maneuvers. The first uses dynamical systems theory in the form of the Cauchy-Green Tensor (CGT). The CGT targeting algorithm leverages an understanding of the maneuver size and direction that best maintains the perturbed orbit near the virtual reference and is developed with a focus on a target only one revolution ahead. The second method applies crossing control to the NRHO stationkeeping problem. By targeting a single component of the virtual reference,  $v_x$ , at the  $xz$ -plane crossing several revolutions downstream, the NRHO is maintained nearby the virtual reference. Neither approach forces a return to the reference path; both allow the spacecraft to simply shadow the reference.

### Short Horizon Maneuvers: CGT Targeting

Dynamical systems theory is introduced with the goal of producing low-cost stationkeeping maneuvers while reducing the demand for computational resources. To explore the capability of a maneuver vector,  $\Delta\mathbf{V}$ , at the current time to influence the path at a later time, consider the evolution of initial variations. Varying the maneuver vector,  $\Delta\mathbf{V}$ , both in direction and/or magnitude will naturally modify the resulting state at the final time. The final time,  $t_f$ , may be defined as a fixed epoch, or as a horizon that recedes as the maneuver time advances. In a phase space (i.e., a space generally comprised of state variables), the variations in the final conditions typically describe a region of attainable states. In other words, assuming an initial variation in terms only of velocity (i.e., a  $\Delta\mathbf{V}$  vector) within some bounded magnitude, the state variations downstream are also bounded. The boundaries downstream reflect the attainable region. Assume that a region of attainable states is traceable to a known geometry. The boundaries for the attainable region can be constructed from linear or nonlinear propagation of the variations. Any knowledge concerning the attainable region geometry may then be employed to determine an initial maneuver that targets a desired final condition.

A description of the attainable region geometry follows from continuous mechanics theory as applied to trajectory design. Concepts that are native to continuous mechanics can facilitate the analysis of solutions in the vicinity of a reference path, especially within the context of non-autonomous systems, such as an  $N$ -body ephemeris model.<sup>35</sup> From this perspective, the dynamical flow nearby a baseline path may be described as the stretching of a fictitious material volume over a given time interval. The stretching for the material volume is mathematically rendered by the Cauchy-Green Strain Tensor, or simply Cauchy-Green Tensor (CGT). The CGT, that is,  $C$ , is the product of the transpose of the STM with itself,<sup>36</sup>

$$C(t_f, t_0) = \Phi^T(t_f, t_0)\Phi(t_f, t_0) \quad (6)$$

where  $t_0$ , and  $t_f$  denote the fixed initial and final epochs. The STM,  $\Phi$ , is essentially a linear mapping of the final perturbation vector,  $\delta\mathbf{x}(t_f)$ , given a variation of the initial conditions,  $\delta\mathbf{x}(t_0)$ , such that

$$\delta\mathbf{x}(t_f) = \Phi(t_f, t_0)\delta\mathbf{x}(t_0) \quad (7)$$

The CGT is a squaring operation that returns the relationship between the initial and final distance from the nominal motion

$$\|\delta\mathbf{x}(t_f)\|^2 = \delta\mathbf{x}(t_0)^T C(t_f, t_0)\delta\mathbf{x}(t_0) \quad (8)$$

The distance  $\|\delta\mathbf{x}(t_f)\|^2$  reveals the growth or the decay of the initial vector perturbation. Furthermore, the eigendecomposition of the CGT allows identification of the principal directions of expansion for the dynamical flow, including those that are locally associated with the largest and smallest stretching. The CGT is – by definition – a positive definite matrix; when computing eigenvalues and eigenvectors, it is, therefore, better behaved than the corresponding STM. Note,  $\lambda_i$  and  $\xi_i$  are the eigenvalues and eigenvectors of the tensor. Accordingly, within a linear approximation, the local phase space expands or contracts in the direction  $\xi_i$  by a factor  $\sqrt{\lambda_i}$ , as

$$\|\Phi(t_f, t_0)\xi_i\| = \sqrt{\lambda_i}\|\xi_i\| \quad (9)$$

Consider a spherical region in the phase space nearby the initial state. As the initial variation evolves, regard this region as a physical continuum that translates and rotates in time along the path, but also undergoes local deformation. Within a linear approximation, Eq. (9) describes a continuum that contracts or expands while maintaining an ellipsoidal shape, as in Figure 7. The principal directions,  $\xi_i$ , may be mapped to the final time

as  $\Phi(t_f, t_0)\xi_i/\|\xi_i\|$  and, thus, describe the ellipsoid axes; the ellipsoid size along each axis is derived from the rates of expansion and contraction,  $\sqrt{\lambda_i}$ , as  $\sqrt{\lambda_i}\|\xi_i\|$ . The CGT and its eigendecomposition enable a linear approximation for the attainable region nearby a reference, such as that in the proposed stationkeeping strategy.

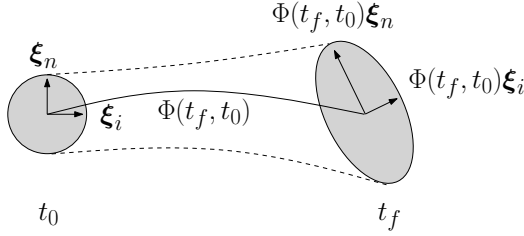


**Figure 7:** Stretching associated with eigenvectors of the Cauchy-Green tensor.

Within this stationkeeping algorithm, a maneuver typically targets an arbitrary point,  $\mathbf{x}_T$ . Focusing on this objective only, and assuming an attainable region,  $\mathcal{E}$ , that is fixed by the size of a maneuver,  $\Delta V_M$ , the most desirable final condition is, naturally, the point within the attainable region  $\mathbf{x} \in \mathcal{E}$  that is closest to target,  $\mathbf{x}_T$ . Note, bolded quantities refer to vectors, while unbolded quantities refer to vector magnitudes. A linear approximation for the final region that is accessible via the current value  $\Delta V_M$ , is constructed as an  $n$ -dimensional ellipsoid

using the eigenstructure for the CGT corresponding to the uncontrolled nominal trajectory is given as

$$\mathcal{E} = \{\mathbf{x} | (\mathbf{x} - \mathbf{c})^T Q (\mathbf{x} - \mathbf{c}) = 1\} \quad (10)$$

where  $\mathbf{c}$  is the center of the ellipsoid and  $Q = U\Sigma U^T$  is a symmetric, positive definite matrix. The center of the ellipsoid lies at the uncorrected final state,  $\mathbf{c} = \mathbf{x}_U$ . The principal axes of the ellipsoid are defined along the directions  $\mathbf{u}_i = \frac{\Phi(E_T, E_M, \mathbf{x}_M)\xi_i}{|\Phi(E_T, E_M, \mathbf{x}_M)\xi_i|}$ , which form the matrix  $U = [\mathbf{u}_1, \mathbf{u}_2, \dots, \mathbf{u}_N]$ . The matrix  $\Sigma$  is diagonal, with elements equal to the inverse-square of the ellipsoid radii,  $1/\rho_i = 1/(\sqrt{\lambda_i}\Delta V_M)^2$ . Determining the location within the ellipsoidal attainable region,  $\mathbf{x}^*$ , that is closest to the target state,  $\mathbf{x}_T$ , i.e.,

$$\mathbf{x}^* = \arg \min_{\mathbf{x} \in \mathcal{E}} \|\mathbf{x} - \mathbf{x}_T\|^2 \quad (11)$$

is equivalent to solving a geometric problem. To meet the desired target tolerance,  $\epsilon_T$ , it may be necessary to adjust the size of the ellipsoid that approximates the final attainable region, and recompute the point  $\mathbf{x}^*$ . Modifying the size of the final region is equivalent to adjusting the size of the initial  $\Delta V_M$ . As illustrated in Figure 8, the straightforward criteria to adjust a maneuver size is to modify  $\Delta V_M$ . If the locally optimal solu-

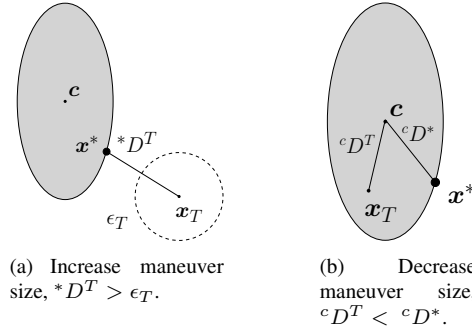


**Figure 8:** Attainable region adjustment schematics.

tion  $\mathbf{x}^*$  is further from the target than the desired tolerance an increase in  $\Delta V_M$  is recommended; in contrast, a maneuver size is reduced, if the target point is already inside the attainable region. After a maneuver size is selected, the closest point to the target at the final time is also defined by

$$\frac{1}{\Delta V_M}(\mathbf{x}^* - \mathbf{c}) = \begin{bmatrix} \Phi_{rv} \\ \Phi_{vv} \end{bmatrix} \frac{\Delta V_M}{\|\Delta V_M\|} = A \frac{\Delta V_M}{\|\Delta V_M\|} \quad (12)$$

Inverting Eq. (12) enables, in principle, determination of the appropriate direction,  $\Delta V_M/\Delta V_M$ , corresponding to the initial corrective maneuver. However, Eq. (12) describes an overdetermined system. One

option, is to compute the initial maneuver direction as the least squares solution of the system in Eq. (12), i.e.,

$$\frac{\Delta \mathbf{V}_M}{\|\Delta \mathbf{V}_M\|} = \frac{1}{\Delta V_M} (A^T A)^{-1} A^T (\mathbf{x}^* - \mathbf{c}) \quad (13)$$

The solution of Eq. (13) completes the information required to compute the vector,  $\Delta \mathbf{V}_M$ , that renders a stationkeeping maneuver. From experimentation, if the final maneuver size,  $\Delta V_M$ , is larger than 1 m/s, the maneuver prediction from Eq. (13) may be inaccurate for application to an  $L_2$  NRHO within the Earth-Moon system. The linear approximation for the motion becomes less precise for a large  $\Delta V_M$ . For the same reason, caution is required in adopting this algorithm, as currently formulated, in combination with a long time of flight. For a cost-efficient long-term mission, the number of large maneuvers must be limited. Additionally, a conservative design may require frequent maneuvers to increase confidence in spacecraft navigation measures. A linear approximation for the attainable region, through the CGT, is reasonable for a mission with small, frequent maneuvers. It is possible to extend the CGT targeting algorithm to a long time of flight or large maneuver size by updating the formulation for the attainable region to include nonlinear deformations.

An algorithm that simulates SH maneuvers by incorporating a geometrical approximation for the attainable region to determine correction burns through CGT targeting is constructed as follows.

1. **Formulate input:** From the converged LH baseline, patch point state variables within the ephemeris model,  $\mathbf{X}_{J2000}$ , and the corresponding epochs,  $\mathbf{E}_{J2000}$ , are the input for the SH level in the two-phase stationkeeping approach.
2. **Generate targets:** A list of target state variables and epochs is generated. Possible target events are a crossing of a plane, a trajectory apsis relative to an attracting body, or a fixed time of flight.
3. **Apply OD errors:** Apply Orbit Determination (OD) errors to the current orbital state. OD errors are applied in both position and velocity. An OD error vector,  $\mathbf{e}$ , is added to the current state vector

$$\tilde{\mathbf{x}} = \mathbf{x} + \mathbf{e} \quad (14)$$

assuming that, each entry for the OD error vector,  $\mathbf{e}$ , is stochastic, and is modeled as a Gaussian distribution with zero mean and a given standard deviation. Additionally, errors among different state vector components are assumed to be uncorrelated.

4. **Apply maneuver:** If a maneuver is pre-planned for the current state, it is now applied. A maneuver is represented as an impulsive  $\Delta \mathbf{V}$  vector, which incorporates information for both the thrusting direction and magnitude. The maneuver implementation also includes an additional error,  $e_{\Delta V}$ , on the  $\Delta V$  magnitude. Currently, the maneuver direction is not perturbed. If there is no maneuver planned for the current state, or to mimic a missed burn, consider  $\Delta V = 0$ , and move directly to the next step.
5. **Propagate:** Propagate the current state to the next maneuver event. Common maneuver events include crossing a virtual plane, apse conditions relative to an attracting gravitational body, or surpassing a threshold for an escape warning. Record the state variables vector,  $\mathbf{x}_M$ , and the epoch,  $E_M$ , for the maneuver event.
6. **Select target:** Select the next target from the target list. This selection includes the definition of a target state variable vector,  $\mathbf{x}_T$ , and a target epoch,  $E_T$ , such that  $E_T > E_M$ .
7. **Compute next maneuver:** At a maneuver event, the correction burn, described by the vector  $\Delta \mathbf{V}_M$ , is computed by employing Eq. (13).
8. **Repeat:** Return to step 3 where the current state vector is now  $\mathbf{x}_M$  and the current epoch is now  $E_M$ . Repeat for each revolution.
9. **Deliver output:** The output is a series of maneuvers characterized by the corresponding state variables, epoch, maneuver size, and direction. This information renders the controlled trajectory path within the context of the ephemeris model.

Approximating the region that is attainable via an SH maneuver as an  $n$ -dimensional ellipsoid allows for the formulation of the stationkeeping problem as a geometrical problem. Solutions of this geometrical problem generally demand few computational resources, which may be beneficial for on-board implementation. Present limitations of the algorithm include the assumption of small maneuvers and shorter times of flight (which is derived from the linear approximation of the motion in the vicinity of the current path). When

applied within the ephemeris model, the selection of target states,  $\mathbf{x}_T$ , and target tolerance,  $\epsilon_T$ , are also important for successfully maintaining the desired motion when perturbations are added.

### Short Horizon Maneuvers: $X$ -axis Crossing Control

A second SH maneuver targeting algorithm implements an  $x$ -axis crossing control scheme to facilitate the exploration of maneuver costs associated with a noisy, crewed spacecraft. Similar approaches have been successfully applied to support halo orbiters at Earth-Moon and Sun-Earth libration points, including ARTEMIS<sup>37,38</sup> and WIND.<sup>39</sup> In the current analysis, an updated algorithm accommodates the different characteristics of the NRHO, including decreased orbital period, increased stability characteristics, and closer proximity to the Moon as compared to the orbits flown by ARTEMIS and WIND.

Assume that the spacecraft has been inserted into a virtual NRHO reference via an LH maneuver. As the spacecraft moves along its orbit, it is affected by the initial insertion error and by continuing spacecraft and orbit determination errors. As the orbit diverges from the desired path, it reaches a specified point in the orbit where an SH maneuver is executed to direct the spacecraft back towards an NRHO. At this point, a differential corrector is employed to compute the  $\Delta V$  required to achieve specified targets further ahead in the orbit. The targeted parameters may be associated with a virtual reference orbit or they may be independent of a reference. The targets may be components of the state vector or other orbital parameters such as perilune altitude, time, or osculating orbital elements. An effective strategy for NRHO stationkeeping depends on several variables, including the location and timing (or phasing) of the targeting maneuvers, the specific constraint targets, and the geometrical locations along an orbital revolution as well as the distance downstream to target the selected constraints.

**Maneuver Placement.** The orbit maintenance costs associated with an  $x$ -axis crossing algorithm depend on the frequency and location of SH maneuvers along the NRHO. The ARTEMIS and WIND algorithms each apply multiple orbit maintenance maneuvers per revolution. However, the NRHO is characterized by a shorter period and slower divergence as compared to the ARTEMIS and WIND trajectories. Both once-per-revolution and twice-per-revolution maneuvers are investigated, with varying locations along the orbit considered. Adding the option of a second SH maneuver per revolution is not observed to reduce stationkeeping costs. In fact, depending on the magnitude of the errors, in many cases, a maneuver is not necessary every revolution. Thus, in the current analysis, a single SH maneuver is planned for each revolution.

The selection of the SH maneuver location depends on the sensitivity of the orbit to perturbations at various locations along the orbit. The NRHO is highly sensitive to perturbations near perilune. While a maneuver placed at or near perilune has an increased potential to influence the trajectory downstream, navigation and maneuver execution errors are associated with each maneuver. When these errors are incorporated during a maneuver at perilune, they significantly perturb the NRHO and result in increased stationkeeping costs and reduced algorithm robustness. Due to the sensitivity of the trajectory near perilune, events such as orbit insertion, stationkeeping maneuvers, and other perturbations near perilune are avoided. The relationship between annual stationkeeping costs and maneuver placement is visualized in Figure 9 for six sample NRHOs with perilune radii ranging from 2100 to 6500 km. For each case represented, a fixed set of navigation and space-

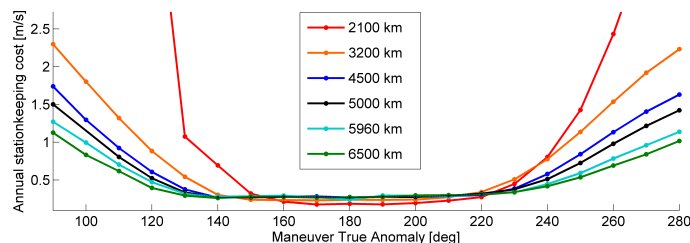


**Figure 9:** Annual stationkeeping  $\Delta V$  cost vs. maneuver placement within the orbit for a quiet-spacecraft configuration for six reference NRHOs.

craft errors is applied to a spacecraft over 50 revolutions. Not surprisingly, the NRHOs with closer perilune passages are more sensitive to the maneuver location than are those with higher values of  $r_p$ . For  $x$ -axis

crossing control, a maneuver location within 30 degrees of apolune appears to be most favorable given the current formulation. For simplicity, the SH maneuvers are placed at apolune.

**Constraint targets.** Several combinations for constraint targets are investigated. Potential targets include position and velocity components as well as perilune passage time and perilune radius. The  $x$ -axis crossing control algorithm can target to a virtual LH reference orbit or to independent quantities. In a periodic NRHO in the CR3BP, the  $x$  and  $z$  components of rotating velocity are both equal to zero at the  $xz$ -plane crossings. It is, thus, reasonable to consider targeting  $v_x$  and/or  $v_z$  with a goal that the values are equal to zero at one of the plane crossings. Such an algorithm combines LH and SH analysis into a single step. Targeting solely  $v_z = 0$  is not sufficient. Targeting  $v_x = 0$  at the  $xz$ -plane crossing is effective, but it requires a longer targeting horizon to achieve low stationkeeping costs. The longer horizon is associated with increased computation time and reduced robustness to large errors. Alternatively, the LH and SH analyses are separated, and an algorithm is selected that targets a virtual LH reference.

The lowest observed stationkeeping costs and highest rates of success (algorithm robustness) are achieved by implementing a simple algorithm that applies a maneuver at apoapsis to target a rotating  $x$ -velocity equal to a value along the reference trajectory. Including constraints on perilune radius or perilune passage time tends to increase stationkeeping costs without increasing algorithm robustness. Targeting additional position or velocity components corresponding to an LH reference point can result in closer adherence to the reference itself, but can also significantly increase the stationkeeping cost. The focus on the rotating  $x$ -velocity alone mirrors the operational stationkeeping algorithms employed by ARTEMIS and WIND.

**Target Location.** Finally, the downstream location of the target  $x$ -velocity,  $v_x$ , is adjusted to improve performance. Perilune, apolune, and the  $xz$ -plane crossings near the apse points are investigated. In the  $x$ -axis crossing control algorithm, placing the target at perilune or the nearby  $xz$ -plane crossing is observed to result in a lower cost than placing the target at or near apolune. Another significant influence on the stationkeeping cost is the length of the receding horizon for targeting. With a maneuver placed at apolune,  $v_x$  can be targeted one half revolution ahead at the following perilune. If the targeting horizon is extended, however, the cost for each maneuver can be significantly reduced. By targeting ahead 2.5 revolutions, the cost is reduced by a factor of 4. Targeting further ahead continues to reduce the stationkeeping cost, but the computation time is increased. In addition, when the errors applied to the spacecraft are large, a longer horizon can lead to difficulties converging on a solution. This trade-off occurs when the horizon is longer than the number of revolutions that an uncontrolled spacecraft reliably remains in the NRHO vicinity without escape or impact. Therefore, a compromise to balance cost, computation time, and reliability is necessary. In the current study, a receding horizon equal to approximately 6.5 revolutions is selected. If the targeter is unable to converge, the horizon is reduced to 4.5 revolutions. If further convergence failures are encountered, the horizon is further reduced to 2.5 revolutions; finally, half a revolution offers the targeter the best chance to converge on a low-cost solution. A plot of the annual stationkeeping cost vs. targeting horizon appears in Figure 10 for four reference NRHOs with low-level orbit determination errors and a quiet spacecraft configuration, as defined in Table 1. Each data point represents the mean annual  $\Delta V$  for 100 Monte Carlo trials with 50 revolutions

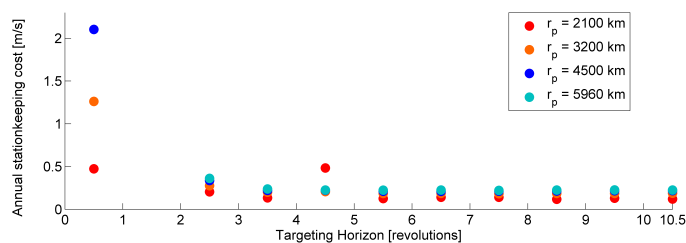


**Figure 10:** Annual stationkeeping  $\Delta V$  cost vs. targeting horizon for 100 Monte Carlo trials with a quiet-spacecraft configuration for four reference NRHOs.

per trial. For each reference NRHO, targeting half a revolution ahead to the next perilune is effective but expensive. At a horizon distance equal to 1.5 revolutions, the algorithm is currently observed to be ineffective. However, the stationkeeping costs begin to come down with a horizon of 2.5 revolutions and longer. At a

horizon length of 5.5 revolutions, the costs are consistently low for the cases investigated in this analysis.

**Additional Tuning Parameters.** In addition to target selection and maneuver placement, several other tuning parameters influence the cost of orbit maintenance. One notable example is the tolerance on the targeted parameter. If the tolerance on  $v_x$  is too tight, the orbit will be overconstrained, and the stationkeeping  $\Delta V$  will be unnecessarily high. If the tolerance is too loose, the trajectory will stray too far from the reference, resulting in higher cost to return to a nearby orbit in subsequent revolutions. A tolerance of 0.45 m/s is selected for the current analysis. A second tuning parameter that affects the stationkeeping cost is the maximum allowed maneuver magnitude. If the maximum  $\Delta V$  is too low, the targeter will not consistently be able to converge on a solution, leading to an increased number of failure cases in Monte Carlo analyses. If the maximum  $\Delta V$  is too high, on the other hand, the targeter may converge on unnecessarily high stationkeeping maneuvers, leading to a higher total cost. The effects of the maximum allowable maneuver size are particularly noticeable in cases with large orbit determination errors. The maximum allowed maneuver magnitude in the current analysis ranges from 5 to 20 m/s per axis, depending on the selected NRHO and the errors that are incorporated.

No optimization is applied to the maneuver computation strategy in this current approach. Rather, a feasible solution is achieved by varying the three components of the impulsive  $\Delta V$ . In both the ARTEMIS and WIND mission operations, the optimal maneuver direction was observed to align with the stable mode along the halo orbit.<sup>38,39</sup> This fact led to the reduction of stationkeeping  $\Delta V$  without requiring optimization for every maneuver. However, constraining the maneuver direction to align with the stable mode along the NRHO in  $x$ -axis crossing control has not led to an observable reduction in stationkeeping cost. Due to the nearly linearly stable nature of the NRHO, the stable mode is not well defined and, therefore, the stable eigenvector of the monodromy matrix of the NRHO may not supply useful directional information. Instead, the Cauchy-Green tensor provides such dynamical information for stable and nearly-stable NRHOs.

**Algorithm.** The stationkeeping process applied in the  $x$ -axis crossing control analysis is straightforward. The steps are summarized as follows:

1. **Formulate input:** A state from the converged LH reference orbit in the ephemeris model,  $\mathbf{X}_{J2000}$ , and the corresponding epoch,  $E_{J2000}$ , supplies the initial conditions for the SH level of the two-phase stationkeeping approach.
2. **Generate target list:** At each  $xz$ -plane crossing near perilune, the rotating  $v_x$  value is recorded from the LH reference to serve as a target for the perturbed spacecraft over the duration of the simulation.
3. **Apply insertion error:** Compute the insertion error and apply it to the position and velocity vectors at the spacecraft apolune as described in Eq. (14).
4. **Compute error on  $C_r$ :** The percent error on  $C_r$  (solar radiation pressure coefficient) is modeled as a Gaussian distribution with zero mean and the specified standard deviation.
5. **Compute next maneuver:** At a maneuver event, the correction burn, described by the vector  $\Delta \mathbf{V}_M$ , is computed by employing a differential corrector. Using a single-shooting algorithm, the three components of  $\Delta \mathbf{V}_M$  are varied within a set of limits to achieve  $v_x = v_{xref}$  to a specified tolerance at the  $xz$ -plane crossing near periapsis 6.5 revolutions downstream. No errors are included in the propagation during targeting.
6. **Reduce targeting horizon:** If the targeter fails to converge, reduce the horizon to 4.5, 2.5, or 0.5 revs ahead, as required. If the targeter still fails to converge, mark the case as failed and exclude the case from the set.
7. **Apply navigation and SRP errors:** Compute the orbit determination error and apply it to the pre-maneuver position and velocity states at the spacecraft apolune as described in Eq. (14). The percent error on SRP area is modeled as a Gaussian distribution with zero mean and the specified standard deviation. Apply the  $C_r$  error and SRP area error to the spacecraft characteristics.
8. **Add maneuver to spacecraft state:** If the computed  $\Delta V_M$  is greater than the minimum threshold, maneuver the spacecraft using the computed  $\Delta \mathbf{V}_M$ , perturbed by the computed maneuver execution error. If the targeted  $\Delta V_M$  is smaller than the minimum threshold, skip the maneuver.
9. **Propagate spacecraft:** Propagate the spacecraft to the next apolune. If noisy-spacecraft errors are included in the simulation, the integration is stopped at each specified interval. Each of the noisy-

spacecraft error types is modeled with a fixed magnitude and random direction. A  $\Delta V$  corresponding to the computed error is applied to the spacecraft and the integration is restarted, repeating until apolune is reached.

10. **Repeat:** Return to Step 5 and repeat for each revolution.
11. **Deliver output:** The output is a series of maneuvers characterized by the corresponding state variables, epoch, maneuver size, and direction.

The  $x$ -axis crossing control algorithm computes a set of SH maneuvers designed to maintain a spacecraft within an NRHO for an extended duration. The simple yet robust algorithm allows for analysis of the effects on stationkeeping cost of various errors associated with both noisy and quiet spacecraft configurations.

## APPLICATION: EARTH-MOON SOUTHERN HALO FAMILY IN A HIGHER-FIDELITY MODEL

Stationkeeping algorithms to sustain a southern NRHO-like motion are examined within a higher-fidelity model based on the Earth-Moon system. Both LH and SH maneuvers are simulated, however, the analysis of SH maneuvers is prioritized at the current state of the investigation. In this stationkeeping investigation, the CGT targeting approach is examined to maintain an orbit with a focus on targets that are only one revolution or less downstream. An  $x$ -axis crossing control strategy employs targets that are generally at least 6 revolutions ahead. Both can be successful as demonstrated by the results.

### Navigation and Spacecraft Error Models

In each of the stationkeeping simulations, orbit determination errors of 1 km in position and 1 cm/s in velocity ( $3\sigma$ ) are assumed. For some simulations, perturbations associated with the spacecraft itself are also incorporated. Two spacecraft configurations are investigated: a quiet spacecraft configuration (no humans present, no attitude deadbanding required) and a noisy spacecraft setup (humans on board, 3-axis stabilized). These configurations are detailed in Table 1 and Table 2, respectively.

The quiet spacecraft configuration includes solar radiation pressure (SRP) errors and maneuver execution errors in addition to orbit determination errors. Solar radiation pressure is modeled assuming a spacecraft mass of 25,848 kg, a nominal spacecraft area of 50 m<sup>2</sup>, and a nominal coefficient of reflectivity ( $C_r$ ) of two.<sup>40</sup> A 5% error on SRP area ( $1\sigma$ ) and a 10% error on  $C_r$  ( $1\sigma$ ) result in errors in the SRP force calculation. Two maneuver execution error models are investigated: a fixed error model and a percent error model. In the fixed model, a maneuver execution error of 0.03 cm/s is assumed, applied in a random direction. In the percent error model, a 1% error ( $1\sigma$ ) is applied to the maneuver magnitude. In all cases, a minimum maneuver threshold of 0.15 cm/s is implemented. If a computed  $\Delta V$  is less than the threshold, it is not executed. For a noisy spacecraft inhabited by humans and 3-axis stabilized, additional errors are assumed. The noisy spacecraft errors are included in addition to orbit determination errors and quiet spacecraft errors. These errors include mismodeling of attitude deadband and slew maneuvers, as well as CO<sub>2</sub> expulsion (PSA puffs) and urine dumps. At this time, no *a priori* modeling of the PSA puffs or urine dumps is assumed.

**Table 1:** Quiet spacecraft configuration

Quiet spacecraft errors		
Maneuver Execution (fixed)	0.03 cm/s	fixed, random direction
Maneuver Execution (percent)	1%	$1\sigma$ , 0 mean, Gaussian
SRP Area	5%	$1\sigma$ , 0 mean, Gaussian
$C_r$	10%	$1\sigma$ , 0 mean, Gaussian

**Table 2:** Noisy Spacecraft Configuration

Noisy spacecraft errors. Fixed magnitude, random direction.		
Error Type	magnitude (m/s)	frequency
PSA Puffs	8.3480E-4	every 10 min
Attitude deadbands	2.0043E-5	every 70 min
Attitude slews	6.9751E-4	every 3.2 hours
Urine dumps	1.8840E-3	every 3.0 hours

## Monte Carlo Analysis: CGT Targeting

Propagation of the motion in an ephemeris model is initiated by an LH maneuver. This maneuver is constructed using a CR3BP periodic orbit as a virtual baseline; the current analysis focuses on NRHOs that are members of the southern branch of the  $L_2$  halo family. Sample trajectories for different perilune altitudes that result from a single, initial LH maneuver are plotted in Figure 11 as they appear when corrected in an Earth-Moon-Sun-Jupiter (EMSJ) ephemeris model. For NRHO trajectories that are propagated in an ephemeris model, the perilune altitude may vary visibly; the values for the perilune radius derived from the CR3BP are used solely for convenience in labeling an NRHO motion.

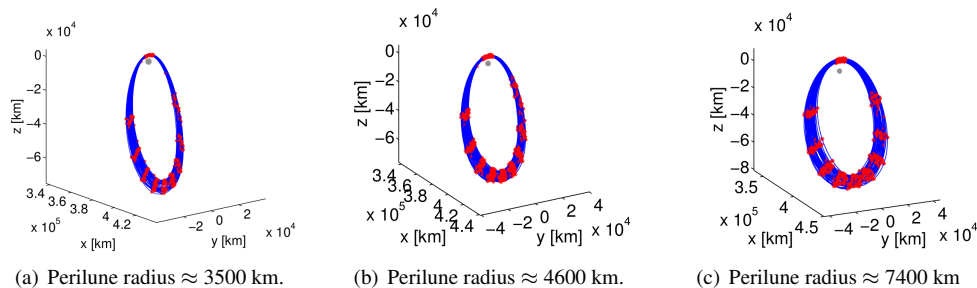


**Figure 11:** NRHO orbits within the Earth-Moon-Sun-Jupiter ephemeris model propagated for 50 revolutions. Initial epoch: 23 November 2020. Patch points are indicated by red stars; the correction process uses 10 patch points per revolution.

Short horizon maneuvers, computed using a CGT targeting scheme, are simulated in the EMSJ ephemeris model, and are effective at sustaining NRHO motion within the higher-fidelity model of a mission environment. As currently formulated, the CGT targeting strategy targets a state defined on the following revolution. Maneuvering on each revolution may enable larger safety margins for the crew and more reliable navigation. A Monte Carlo analysis for a series of 45 SH burns supplies a basis to explore the efficacy of the SH level within the stationkeeping scheme. An NRHO-like baseline trajectory is defined after an LH maneuver is successfully computed (possible baseline paths for the SH level are, for example, those depicted in Figure 11). The SH maneuvers are executed at apolune and target a nominal J2000 position and velocity vector for the subsequent apolune within a tolerance of 0.02 nondimensional units. Expressed in velocity units, such a tolerance is approximately equal to 2 cm/s within the Earth-Moon system. Stochastic, Gaussian distributed errors in each position and velocity component are added along the trajectory as described in Eq. (14). To numerically sample the pool of possible outcomes, with the inclusion of orbital perturbations that are modeled stochastically, the series of 45 SH maneuvers is repeated 500 times for each selected NRHO orbit. The complete set of 500 trials yields a set of results from this Monte Carlo analysis. The total  $\Delta V$  for a series of 45 SH maneuvers is averaged over the 500 trials, and supplies an estimate for the stationkeeping cost for the particular NRHO studied. A series of 45 burns approximately corresponds to a time duration from 300 days to 375 days, depending on the nominal orbit period. The time span is, then, sufficiently large to estimate the annual stationkeeping cost, i.e.,

$$\Delta V_{yr} = \Delta V_{MC} \frac{365[\text{days}]}{\Delta t_{MC}[\text{days}]} \quad (15)$$

where  $\Delta t_{MC}$  is the elapsed time in days that is covered by the Monte Carlo trial.

The results of the Monte Carlo analysis are summarized in Table 3. The first column defines the reference NRHO motion using the nominal CR3BP perilune radius as a label; the second column lists the stochastic error levels for orbit determination; the third column delineates the percentage of the correction burns that are successfully computed over the 45 maneuvers per 500 trials (the success rate indicates the capability for the algorithm to consistently produce a workable solution); the fourth column is the time of flight that approximately corresponds to a series of 45 maneuvers for each reference orbit; the fifth column contains the total  $\Delta V$  for a series of 45 maneuvers, a value that is the average over the Monte Carlo trials; and, the last column displays the stationkeeping cost by linearly projecting the  $\Delta V$  cost over a one year interval using Eq. (15). For the selected NRHOs and orbit determination errors, the SH algorithm never fails within the

randomly generated sample, and annual cost for SH maneuvers is below 10 m/s.

**Table 3:** Annual SH  $\Delta V$  cost for five NRHOs targeted one revolution ahead with CGT Targeting

Perilune radius [km]	OD errors ( $3\sigma$ ) [km,cm/s]	Success rate [%]	Elapsed time [days]	Total $\Delta V$ (average) [m/s]	Projected yr. cost [m/s]
3500	[1,1]	100	300	1.99	2.42
4600	[1,1]	100	318	3.34	3.83
6000	[1,1]	100	337	2.40	2.59
7400	[1,1]	100	356	1.88	1.93
9000	[1,1]	100	375	1.97	1.92

### Monte Carlo Analysis : $X$ -axis Crossing Control

To explore the effects of spacecraft errors on NRHO stationkeeping costs, a similar set of Monte Carlo analyses is performed using  $x$ -axis crossing control. Recall that the  $x$ -axis crossing control stationkeeping scheme focuses on a target state that is 6 or more revolutions downstream. The EMSJ ephemeris model is employed including an 8x8 gravity field for the Moon. Each of six NRHOs is investigated over 500 Monte Carlo trials, each of a duration equal to 50 revolutions. The analyses are run with both the quiet-spacecraft configuration and the noisy-spacecraft configuration, as defined in Tables 1 and 2. The results appear in Table 4 for both the quiet-spacecraft configuration and the noisy-spacecraft configuration. In each case, a targeting horizon of 6.5 revolutions yields 100% success. The average  $\Delta V$  is recorded for the duration of the simulation and annualized according to Eq. (15). Not surprisingly, the costs of stationkeeping a noisy

**Table 4:** Annual SH  $\Delta V$  cost for six NRHOs targeted 6.5 revolutions ahead with  $x$ -axis crossing control

Perilune radius [km]	OD errors ( $3\sigma$ ) [km,cm/s]	Success rate [%]	Elapsed Time [days]	Quiet: Total $\Delta V$ (average) [m/s]	Quiet: Projected yr. cost [m/s]	Noisy: Total $\Delta V$ (average) [m/s]	Noisy: Projected yr. cost [m/s]
2100	[1,1]	100	304	0.11	0.13	0.92	1.10
3200	[1,1]	100	329	0.17	0.19	1.14	1.26
4500	[1,1]	100	348	0.20	0.21	1.34	1.41
5000	[1,1]	100	356	0.21	0.22	1.41	1.45
5960	[1,1]	100	370	0.22	0.22	1.56	1.54
6500	[1,1]	100	378	0.23	0.22	1.62	1.56

spacecraft are higher than the costs associated with the quiet spacecraft by about an order of magnitude. For the six NRHOs investigated with  $x$ -axis crossing control, the stationkeeping costs tend to decrease with smaller orbits as reflected by the decreasing perilune radii. Additional cases and trends are explored in Davis et al.<sup>40</sup> As observed with CGT targeting, in each case, the annual stationkeeping costs remain below 10 m/s. Note that the targeting horizon selected in the  $x$ -axis crossing control implementation (6.5 revolutions) suggests that the horizon is an important parameter in NRHO orbit maintenance.

### FINAL REMARKS

To validate the NRHO as a viable candidate orbit for a habitat spacecraft, many factors must be considered. One important component is stationkeeping—maintaining the spacecraft in an orbit long-term at low cost. The current analysis investigates two different strategies that meet different objectives. The CGT targeting approach leverages dynamical systems theory to determine maneuver direction and magnitude to maintain the spacecraft in the NRHO region while using limited computational resources. An  $x$ -axis crossing control implementation facilitates analysis of the effects of spacecraft errors on the stationkeeping costs. The strategies in the current analysis are responsive to the notable characteristics of the NRHO regime—stability, orbital period, and proximity to the Moon—and adapt libration point orbit stationkeeping concepts for application to NRHOs. Both strategies result in robust, low-cost methods to maintain a spacecraft in an NRHO for a long duration for different operational conditions. The analysis offers support, from the orbit maintenance

perspective, for the feasibility of an NRHO as a candidate orbit for a long-term habitat spacecraft. Ongoing studies are exploring several areas. Topics include the effectiveness of the  $x$ -axis crossing control strategy for a shorter targeting horizon, analysis of the maneuver directions computed by the CGT and  $x$ -axis crossing strategies, the incorporation of phasing maneuvers into the stationkeeping process, and the development of a nonlinear description for the attainable region for CGT targeting.

## ACKNOWLEDGMENTS

The authors would like to thank Roland Martinez and Ryan Whitley their support, and David Folta, Jonathan Brown, and Jeremy Petersen for insightful discussions on ARTEMIS and WIND stationkeeping. Portions of this work were completed at NASA JSC and Purdue University through contract #NNJ13HA01C and grant #NNX13AK60A, respectfully.

## REFERENCES

- [1] B. Hufenbach, K. Laurini, N. Satoh, C. Lange, R. Martinez, J. Hill, M. Landgraf, and A. Bergamasco, "International Missions to Lunar Vicinity and Surface - Near-Term Mission Scenario of the Global Space Exploration Roadmap," *IAF 66th International Astronautical Congress*, October 2015.
- [2] K. Laurini, B. Hufenbach, N. Satoh, J. Hill, and A. Ouellet, "The Global Exploration Roadmap and Expanding Human/Robotic Exploration Mission Collaboration Opportunities," *IAF 66th International Astronautical Congress*, October 2015.
- [3] R. Whitley and R. Martinez, "Options for Staging Orbits in Cis-Lunar Space," *IEEE Aerospace 2015*, March 2015.
- [4] C. E. Roberts, "Long Term Missions at the Sun-Earth Libration Point L1: ACE, SOHO and WIND," *Proceedings of the AAS/AIAA Astrodynamics Specialist Conference, AAS Paper*, No. 11-485, August 2011.
- [5] C. L. Bennet, M. Bay, M. Halpern, G. Hinshaw, C. Jackson, N. Jarosik, A. Kogut, M. Limon, S. S. Meyer, L. Page, D. N. Spergel, G. S. Tucker, D. T. Wilkinson, E. Wollack, and E. L. Wright, "The Microwave Anisotropy Probe (MAP) Mission," *Bulliten of the American Astronomical Society*, Vol. 28, 1996.
- [6] M. Lo, B. Williams, W. Bollman, D. Han, Y. Hahn, J. Bell, E. Hirst, R. Corwin, P. Hong, K. Howell, B. Barden, and R. Wilson, "GENESIS Mission Design," *Proceedings of the AAS/AIAA Astrodynamics Specialist Conference, AAS Paper*, Boston, Massachusetts, August 1998.
- [7] D. J. Dichmann and C. M. Alberding, "Stationkeeping Monte Carlo Simulation for the James Webb Space Telescope," *NASA Goddard Flight Mechanics Symposium*, Greenbelt, Maryland, 2006.
- [8] S. B. Broschart, M. J. Chung, S. J. Hatch, J. H. Ma, T. H. Sweetser, S. S. Weinstein-Weiss, and V. Angelopoulos, "Perliminary Trajectory Design for the ARTEMIS Lunar Mission," *Advances in the Astronautical Sciences*, Vol. 135, No. 2, 2009.
- [9] K. Tajdaran, "Incorporation of Mission Design Constraints in Floquet Mode and Hamiltonian Structure-Preserving Orbital Maintenance Strategies for Libration Point Orbits," M.S. Thesis, School of Aeronautics and Astronautics, Purdue University, West Lafayette, Indiana, December 2015.
- [10] K. Howell and J. Breakwell, "Almost Rectilinear Halo Orbits," *Celestial Mechanics*, Vol. 32, No. 1, 1984, pp. 29–52.
- [11] J. Williams, D. E. Lee, R. L. Whitley, K. A. Bokelmann, D. C. Davis, and C. F. Berry, "Targeting Cislunar Near Rectilinear Halo Orbits for Human Space Exploration," No. AAS 17-267, Feb. 2017.
- [12] R. Farquhar, "The Utilization of Halo Orbits in Advanced Lunar Operations," *NASA Technical Note, NASA TN D-6365*, July 1971.
- [13] C. Renault and D. Scheeres, "Statistical analysis of control maneuvers in unstable orbital environments," *Journal of Guidance, Control, and Dynamics*, Vol. 26, No. 5, 2003, pp. 758–769.
- [14] D. Folta and F. Vaughn, "A Survey of Earth-Moon Libration Orbits: Stationkeeping Strategies and Intra-Orbit Transfers," 2004.
- [15] Y. Xu and S. Suman, "Robust stationkeeping control for libration point quasi-periodic orbits," *Journal of Aerospace Engineering*, Vol. 21, No. 2, 2008, pp. 102–115.
- [16] E. Gustafson and D. Scheeres, "Optimal timing of control-law updates for unstable systems with continuous control," *Journal of Guidance, Control, and Dynamics*, Vol. 32, No. 3, 2009, pp. 878–887.
- [17] G. Gómez, J. Llibre, R. Martínez, and C. Simó, "Station keeping of a quasiperiodic halo orbit using invariant manifolds," *Proceed. 2nd Internat. Symp. on spacecraft flight dynamics, Darmstadt*, 1986, pp. 65–70.

- [18] C. Simó, G. Gómez, J. Llibre, R. Martinez, and J. Rodriguez, “On the optimal station keeping control of halo orbits,” *Acta Astronautica*, Vol. 15, No. 6, 1987, pp. 391–397.
- [19] K. Howell and T. Keeter, “Station-keeping strategies for libration point orbits- Target point and Floquet Mode approaches,” *Spaceflight mechanics 1995*, 1995, pp. 1377–1396.
- [20] G. Gómez, K. Howell, J. Masdemont, and C. Simo, “Station-keeping strategies for translunar libration point orbits,” *Advances in Astronautical Sciences*, Vol. 99, No. 2, 1998, pp. 949–967.
- [21] S. Soldini, C. Colombo, and S. Walker, “Comparison of Hamiltonian structure-preserving and Floquet mode station-keeping for Libration-point orbits,” *AIAA/AAS Astrodynamics Specialist Conference, AIAA-2014-4118, San Diego, California*, 2014, pp. 4–7.
- [22] K. Williams, B. Barden, K. Howell, M. Lo, and R. Wilson, “Genesis halo orbit station keeping design,” *International Symposium: Spaceflight Dynamics*, 2000.
- [23] K. Howell and H. Pernicka, “Station-keeping method for libration point trajectories,” *Journal of Guidance, Control, and Dynamics*, Vol. 16, No. 1, 1993, pp. 151–159.
- [24] D. Grebow, M. Ozimek, K. Howell, and D. Folta, “Multibody orbit architectures for lunar south pole coverage,” *Journal of Spacecraft and Rockets*, Vol. 45, No. 2, 2008, pp. 344–358.
- [25] D. Scheeres, F.-Y. Hsiao, and N. Vinh, “Stabilizing motion relative to an unstable orbit: applications to spacecraft formation flight,” *Journal of Guidance, Control, and Dynamics*, Vol. 26, No. 1, 2003, pp. 62–73.
- [26] D. Folta, T. Pavlak, A. Haapala, K. Howell, and M. Woodard, “Earth–Moon libration point orbit station-keeping: theory, modeling, and operations,” *Acta Astronautica*, Vol. 94, No. 1, 2014, pp. 421–433.
- [27] T. Pavlak and K. Howell, “Strategy for long-term libration point orbit stationkeeping in the Earth-Moon system,” *Proceedings of the AAS/AIAA Astrodynamics Specialist Conference, AAS Paper*, No. 11-516, 2011.
- [28] T. S. Shirobokov, M. and M. Ovchinnikov, “Recovery of halo orbit missions in case of contingent station-keeping maneuver delay,” *Advances in Space Research*, 2016.
- [29] D. Folta, T. Pavlak, K. Howell, M. Woodard, and D. Woodfork, “Stationkeeping of Lissajous trajectories in the Earth-Moon system with applications to ARTEMIS,” *Advances in the Astronautical Sciences*, 2010, pp. 193–208.
- [30] D. Rohrbaugh and C. Schiff, “Stationkeeping Approach for the Microwave Anisotropy Probe (MAP),” *AIAA/AAS Astrodynamics Specialist Conference, Monterey, California*, 2002.
- [31] D. Dichmann, C. Alberding, and W. Yu, “Stationkeeping Monte Carlo Simulation for the James Webb Space Telescope,” 2014.
- [32] C. Short, K. C. Howell, A. Haapala, and D. Dichmann, “Mode Analysis for Long-Term Behavior in a Resonant Earth-Moon Trajectory,” *Journal of the Astronautical Sciences*, November 2016, pp. 1–32.
- [33] C. Short, D. Blazevski, K. Howell, and G. Haller, “Stretching in Phase Space and Application in General Nonautonomous Multi-Body Problems,” *Celestial Mechanics and Dynamical Astronomy*, Vol. 122, July 2015, pp. 213–288.
- [34] T. Pavlak, *Trajectory Design and Orbit Maintenance Strategies in Multi-Body Dynamical Regimes*. Ph.D. Dissertation, School of Aeronautics and Astronautics, Purdue University, West Lafayette, Indiana, May 2013.
- [35] C. Short, *Flow-informed Strategies for Trajectory Design and Analysis*. Ph.D. Dissertation, School of Aeronautics and Astronautics, Purdue University, West Lafayette, Indiana, May 2016.
- [36] D. Smith, *An Introduction to Continuum Mechanics – after Truesdell and Noll*. Springer Netherlands, 1993.
- [37] D. Folta, M. Woodard, and D. Cosgrove, “Stationkeeping of the First Earth-Moon Libration Orbiters: The ARTEMIS Mission,” *AAS/AIAA Astrodynamics Specialist Conference, Girdwood, Alaska*, August, 2011.
- [38] D. Folta, T. Pavlak, K. Howell, M. Woodard, and D. Woodfork, “Stationkeeping of Lissajous Trajectories in the Earth-Moon System with Applications to ARTEMIS,” *20th AAS/AIAA Space Flight Mechanics Meeting, San Diego, California*, February, 2010.
- [39] J. Petersen and J. Brown, “Applying Dynamical Systems Theory to Optimize Libration Point Orbit Stationkeeping Maneuvers for WIND,” *AAS/AIAA Astrodynamics Specialists Conference, San Diego, California*, August, 2014.
- [40] D. C. Davis, S. A. Bhatt, K. Howell, J. Jang, R. Whitley, F. Clark, D. Guzzetti, E. Zimovan, and G. Barton, “Orbit Maintenance and Navigation of Human Spacecraft at Cislunar Near Rectilinear Halo Orbits,” *Paper No. AIAA-2017-269, AAS/AIAA Spaceflight Mechanics Meeting, San Antonio, Texas*, February, 2017.